Proceedings of the International Conference on Oxide Materials for Electronic Engineering, May 29–June 2, 2017, Lviv

# Synthesis, Properties and Applications of some Magnetic Oxide Based Nanoparticles and Films

A. Belous[a], A. Tovstolytkin[b], S. Solopan[a], Yu. Shlapa[a,*] and O. Fedorchuk[a]

[a]Vernadskii Institute of General and Inorganic Chemistry of the NAS of Ukraine, 03680 Kyiv, 32/34 Palladina Ave., Ukraine

[b]Institute of Magnetism of the NAS of Ukraine and MSE of Ukraine, 34b Vernadskii Blvd., 03680 Kyiv, Ukraine

The work highlights peculiar features of synthesis and summarizes important properties of nanoparticles and films based on two types of oxide magnets: with spinel and perovskite-type structures. The attention is drawn to the differences in the processes underlying the formation of crystalline phase in the materials of each group. It is shown that for the spinels, the formation of weakly agglomerated crystalline nanoparticles can occur in the process of synthesis, but for the perovskite-like magnets, the formation of crystalline nanoparticles requires additional high-temperature treatment. It is demonstrated that synthesized nanoparticles and films may find wide practical applications, particularly as the heat mediators in hyperthermia treatment therapy, as components of left-handed media, ferroelectric-ferromagnetic layered structures and composite microwave resonators. They also may be used as integral parts of composite structures, which possess magnetic-field-controlled properties and display giant magnetocaloric effect.

DOI: 10.12693/APhysPolA.133.1006

PACS/topics: oxide magnets, ferrites, spinel, perovskite, nanoparticles, film, hyperthermia, magnetocaloric effect, left-handed medium, composite UHF resonator

## 1. Introduction

The research interest in magnetic oxide materials significantly increased since the beginning of 2000th. This was mainly connected with the development and investigation of different ferrite-based nanostructures (weakly agglomerated nanoparticles, films, periodical and multilayer structures etc.), which often demonstrated unique properties. Besides, in 2000th mobile communication systems working in microwave (MW) range began rapidly progressing. This required the development of novel SHF ferrites, investigation of the nature of magnetic and dielectric losses, and exploring the possibilities to control them. New classes of oxide magnets with interesting properties, for example, colossal magnetoresistance, appeared at that time [1]. Novel methods of synthesis of epitaxial films (pulsed laser deposition (PLD) method) and nanostructure investigation (transmission electron microscope (TEM), force microscopes) were being implemented [2, 3]. It became apparent that nanoparticles of some magnetic oxides might find practical application in medicine, particularly, for enhancing the sensitivity of diagnostics methods (MRI) [4], and in therapy (hyperthermia treatment, targeted drug delivery etc.) [5, 6].

At present, a number of methods to synthesize various nanoparticles are known [7]. Most of them are suitable for fabrication of magnetic oxide nanoparticles. At the same time, there is no universal method, which is able to satisfy all necessary requirements. One of the important requirements is to obtain nanoparticles with controlled shape and size distribution. Often, to avoid the particles interaction, an additional requirement appears to ensure the possibility of coating particle surface with specific materials. As a result, the choice of the synthesis method depends on a number of factors, such as crystalline structure, chemical composition, necessity to achieve some important electrophysical characteristics (saturation magnetization, coercivity, high-frequency energy dissipation etc.).

This study highlights peculiar features of synthesis and summarizes important properties of weakly agglomerated nanoparticles, films, periodical and multilayer systems based on two groups of magnetic oxides (with the spinel and perovskite structures) and discusses the prospects of their practical application.

## 2. Methods of synthesis and investigation of the properties of magnetic nanoparticles and films

To obtain magnetite nanoparticles via cryochemical method, $FeCl_3$ and $FeCl_2$ were used as starting reagent and sodium hydroxide NaOH as the precipitator. The starting solution was cooled by the liquid nitrogen. To synthesize magnetite nanoparticles from the reverse microemulsions the aqueous solution of $FeCl_3$ and $FeCl_2$ were used. Cyclohexane and butyl alcohol were used as additional surfactants, which did not take part in the micelle formation; bidistilled water was used as the dispersion medium and solvent, concentrated ammonia solution, as the precipitator. Triton X-100, Brij-35 and CTAB were chosen as the surfactants.

Aqueous solutions of $La(NO_3)_3$, $Mn(NO_3)_2$, and $Sr(NO_3)_2$ were used as starting reagents for sol–gel syn-

*corresponding author; e-mail: yuliashlapa@ukr.net

thesis of (La,Sr)$MnO_3$ (LSMO) nanoparticles. Ethylene glycol (EG) and citric acid (CA) were added as gel forming agents. Obtained mixture was heated with stirring to 80 °C and polyesterification reaction took place. Pyrolysis of the gel was done at 200 °C, and the amorphous powder, which formed at this temperature, was heated up to 800 °C. The aqueous solutions of $La(NO_3)_3$, $Mn(NO_3)_2$, $Sr(NO_3)_3$ were starting reagents in the synthesis LSMO from the reverse microemulsions. Triton X-100, CTAB, Brij-35 were used as the surfactant, cyclohexane and butyl alcohol as the additional surfactants, which did not take part in the micelle formation. Bidistilled water was the dispersion medium, and the concentrated ammonia solution was the precipitator.

Based on the synthesized $Fe_3O_4$ and (La,Sr)$MnO_3$ nanoparticles and 0.1% aqueous agarose solution, magnetic fluids were developed with necessary concentration of magnetic phase.

Epitaxial $La_{0.7}Ca_{0.3}MnO_3$ (LCMO) and $La_{0.7}Sr_{0.3}MnO_3$ (LSMO) films were grown at 775 °C by PLD method ($\lambda = 248$ nm, distance to the target 8 cm, energy fluency 1.5 J cm$^{-2}$ for LCMO and 1.7 J cm$^{-2}$ for LSMO) on one-side-polished 4 mm × 4 mm × 0.5 mm substrates $BaTiO_3$ $(001)_{pseudo-cubic}$. Prior to growth, the substrates were annealed for 1 h at 750 °C after setting a 15 Pa flowing oxygen ambient. The film deposition was performed after the heating of the substrate to 775 °C. After deposition, annealing was performed by setting a static 55 kPa oxygen ambient and subsequently reducing the temperature at 5 °C min$^{-1}$ to 700 °C. After waiting 30 min, the heater temperature was reduced to room temperature at 10 °C min$^{-1}$.

(La,Sr)$MnO_3$ films were synthesized via sol–gel method using the colloid gels. Nanoparticles were dissolved with heating in the dilute 25% nitric acid solution and citric acid was added as the complexing agent. A 50% excess of citric acid and ethylene glycol, based on the amount of moles of the soluble substance, was added to the solution. The solution was kept at a temperature of 80 °C. Than it was cooled and the Triton X-100 surfactant was added to prepare 10% solution. This solution was homogenized for 1 h. Obtained solution was applied on the substrate in several layers using Spin coater SCI-20 device. The intermediate drying the every layer was performed at 120 °C. Sunthesized films were treated at different temperatures (200–1000 °C) in air for 1 h.

Synthesized nanoparticles and films were characterized by XRD analysis using DRON-4 diffractometer (Cu $K_\alpha$ radiation).

Particles size and morphology were analyzed by transmission electron microscope (TEM) JEOL JEM-1400. Particle size distributions were obtained using software packages Image Tool 3 and OriginPro 8.5 SR1 and calculations were done as described in [8].

To estimate the specific loss power (SLP), the ferromagnetic fluids based on the synthesized nanoparticles were placed into the coil (5 turns, diameter 300 mm) that provided the alternating (AC) magnetic field with the frequency (100–400) kHz and field strength up to 9.5 kA/m. The measurements were done according to method described in [9].

Film morphology was studied with a Digital Instruments Nanoscope III atomic force microscope (AFM) operated in tapping mode. Ferromagnetic resonance (FMR) measurements were performed using an X-band ELEXSYS E500 EPR spectrometer, operated at 9.44 GHz. Measurements were carried out in the temperature range of 171–210 K with the applied magnetic field perpendicular to the film plane. This measurement configuration separates resonances in magnetic films from sharp *resonances* due to defects in substrates.

## 3. Properties of synthesized magnetic nanoparticles and films

### *3.1. Properties of magnetic nanoparticles*

During the synthesis of magnetic (La,Sr)$MnO_3$ nanoparticles with the perovskite structure via sol–gel method the high-temperature treatment ($T$ = 873–1073 K) is necessary and it leads to the formation of so-called "bridge bonds" between particles (Fig. 1a). At the same time, weakly agglomerated (La,Sr)$MnO_3$ nanoparticles are formed after precipitation from the reverse microemulsions and further heat treatment (Fig. 1b).

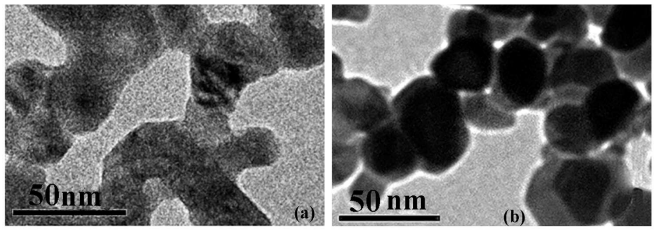


Fig. 1. (La,Sr)$MnO_3$ nanoparticles with the perovskite structure obtained via sol–gel method (a) and by precipitation from reverse microemulsions (b) with further heat treatment at 1073 K.

In contrast to (La,Sr)$MnO_3$ materials with the perovskite structure, crystalline nanoparticles with the spinel structure ($MFe_2O_4$ (M=Fe, Zn, Co, Mn, Ni)) are formed during the synthesis process, independent of the synthesis method (precipitation from microemulsions, cryochemical synthesis, etc.). Weakly agglomerated nanoparticles with small sizes were synthesized ($d \approx$ 4–5 nm) (Fig. 2a,b). The reason for different requirements for crystalline phase formation may originate from the fact that the crystallization energy for the perovskite structure is much higher than that for the spinel structure [10, 11].

The studies demonstrate that synthesized magnetic nanoparticles of both types (with the spinel and perovskite structures) are single-domain and in most cases display superparamagnetic properties. The estimations show that the critical particle size for single-domain state is in the range of 70–126 nm for spinels ($Fe_3O_4$), while

it is near 70 nm for perovskite-like (La,Sr)$MnO_3$ [14]. All synthesized nanoparticles display a maximum on the temperature dependence of magnetization measured in zero-field-cooled mode. The temperature of this maximum is called blocking temperature $T_b$. At room temperature, the nanoparticles are characterized by negligible coercivity.

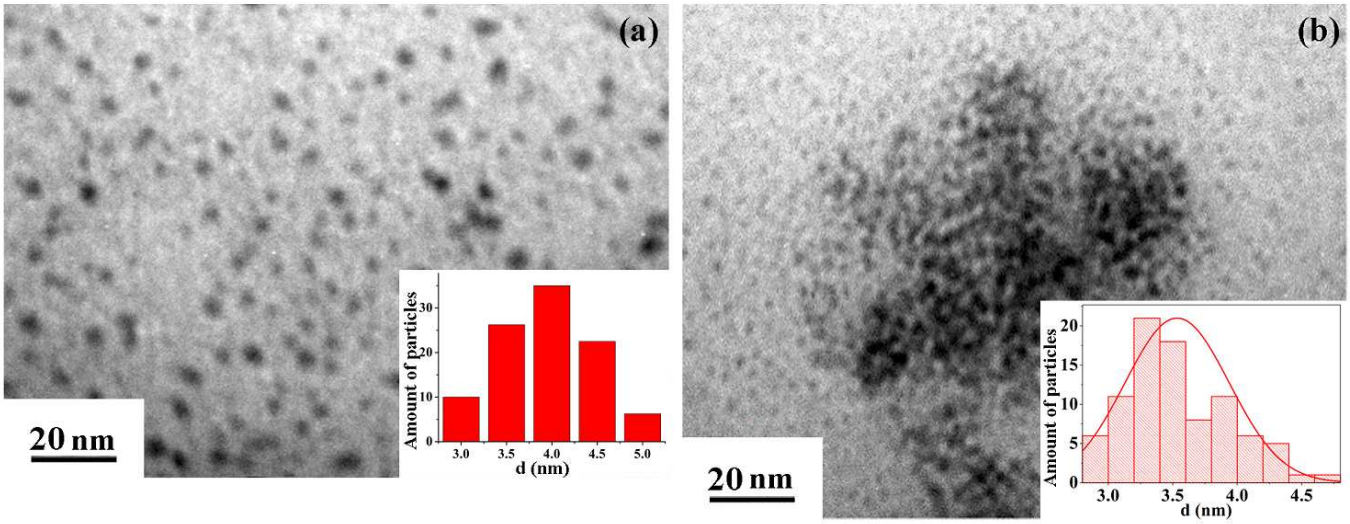


Fig. 2. $Fe_3O_4$ (a) and $CoFe_2O_4$ (b) nanoparticles with the spinel structure obtained by precipitation from microemulsions without further heat treatment.

The investigations show that spinel nanoparticles, which have low blocking temperatures, demonstrate weak heating efficiency under the action of an AC magnetic field (negligible SLP values) (Fig. 3). According to theoretical estimations [15], the heating efficiency of magnetic nanoparticles may be significantly enhanced by finding ways to shift $T_b$ close to room temperature. In this case, the mechanism of high-frequency losses transforms from the Néel–Brown relaxation to the Stoner–Wohlfarth-model-based remagnetization, which results in the strong increase of AC energy dissipation [15]. These data were taken into account for the development of magnetic nanoparticles, which may be used in medicine, particularly in hyperthermia treatment.

### *3.2. Properties of ferromagnetic films*

The surfaces of synthesized $La_{0.7}Ca_{0.3}MnO_3$ and $La_{0.7}Sr_{0.3}MnO_3$ epitaxial films were locally smooth with a roughness of $\approx$ 0.5–1.0 nm, but discontinuous changes of roughness occurred at $BaTiO_3$ twin boundaries. The thickness of films was 34 $\pm$2 nm for LCMO and 55 $\pm$5 nm for LSMO. The investigations showed that the films crystallized in the perovskite structure, lattice parameter for both films in the direction perpendicular to the film plane was 3.81 Å (pseudo-cubic indexation).

$La_{0.7}Sr_{0.3}MnO_3$ films synthesized via sol–gel method using spin coater were applied to the substrate with the rate of 3600 rpm. As electron microscopy data showed, $La_{0.7}Sr_{0.3}MnO_3$ films were homogeneous with the thickness of 250–500 nm. According to the X-ray studied (method of sliding reflection), a crystalline film began to form after the treatment at 600 °C.

## 4. Application of synthesized magnetic nanoparticles and films

### *4.1. Application of magnetic nanoparticles as the mediators in hyperthermia treatment*

Based on the synthesized magnetic nanoparticles with the spinel ($Fe_3O_4$) and perovskite ((La,Sr)$MnO_3$) structures and aqueous agarose solution, magnetic fluids were developed. The investigations of cytotoxicity, genotoxicity, antioxidant activity, and antiviral activity show that $Fe_3O_4$ and (La,Sr)$MnO_3$ nanoparticles in concentrations 0.1–1 mg/ml do not demonstrate any genotoxical activity. In contrast to sol of $Fe_3O_4$ nanoparticles, (La,Sr)$MnO_3$ sol displays the antioxidant activity in concentrations from 0.65 to 5.0 mg/ml: the percentage of living cells was from 94% to 109%, respectively. These data imply that $Fe_3O_4$ and (La,Sr)$MnO_3$ nanoparticles have certain antiviral activity [16]. To determine the therapeutic efficiency of the magnetic fluids based on the synthesized ferromagnetic nanoparticles, the experiments on white rats were carried out. The tumor of Guerin carcinoma was implanted intramuscularly to the rats. After some time magnetic fluid based on (La,Sr)$MnO_3$ nanoparticles was injected into the tumor and this tumor was subjected to the action of AC magnetic field. It was shown that the injection of magnetic fluid with subsequent action of AC magnetic field (frequency 100–400 kHz) resulted in stopping the tumor growth, while the implanted tumor, which was not subjected to such treatment, grew very quickly. The details and results of these experiments are described in [17]. The data imply that the spinel and perovskite-like magnetic nanoparti-

cles are promising materials for the use as the heat mediators in hyperthermia treatment therapy.

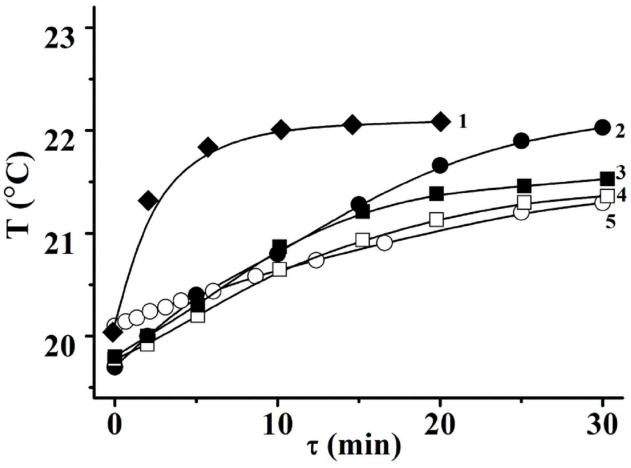


Fig. 3. Temperature of magnetic fluids based on various spinel nanoparticles ($d$ = 4–5 nm) as a function of the time they reside in AC magnetic field with frequency 300 kHz and amplitude 125 Oe: 1 — $ZnFe_2O_4$, 2 — $MnFe_2O_4$, 3 — $Fe_3O_4$, 4 — $CoFe_2O_4$, 5 — $NiFe_2O_4$.

### *4.2. Left-handed media based on (La,Sr)$MnO_3$*

Synthesized oxide magnets are of particular interest for application in engineering, for instance, for creation of the materials with negative refractive index (left-handed media). Such materials were theoretically predicted at the end of 1970th. This novel kind of media is capable of changing a sign of refractive index (along with changes in its value) under magnetic field. A switch to simultaneously negative dielectric and magnetic susceptibilities (a transition to the left-handed state) leads to drastic changes in the propagation of electromagnetic waves both inside the medium and at the boundary with an ordinary (right-handed) material. This gives rise to much broader range of tunability, compared with existing counterparts. The scientific interest to the investigation of the left-handed media is explained by the prospects of their applications in MW technologies, especially in the development of electronically controlled devices for the GHz and THz frequency ranges. One of the most promising objects for creation the left-handed medium in microwave range is perovskite-like (La,Sr)$MnO_3$.

On the one hand, its conductivity changes from semiconducting to metallic upon a transition from paramagnetic to ferromagnetic state. Material with metallic conductivity may display negative values of dielectric susceptibility in the MW range. On the other hand, in the vicinity of ferromagnetic resonance, the negative values of magnetic susceptibility are expected in a certain range of magnetic fields and frequencies. Experimentally, the evidence of left-handed behavior was revealed in a system consisting of one-dimensional photonic crystal terminated by (La,Sr)$MnO_3$ ceramic plate [18]. Photonic crystal was assembled of six to eight double cells consisting of Teflon and quartz. In the presence of external magnetic field ($\approx$ 7 kOe), the field-sensitive transparency peak was observed in the photonic crystal forbidden zone, indicating left-handed behavior of manganite in millimeter waveband [19]. In addition, it was demonstrated [20] that the prism made of (La,Sr)$MnO_3$, which was placed in the waveguide and subjected to the action of a certain magnetic field, refracted electromagnetic wave in the direction that corresponded to the left-handed medium. This experiment is a direct confirmation of the fact that materials (ceramics, films) based on (La,Sr)$MnO_3$ may display left-handed behavior in MW range under the action of purposely chosen external magnetic field.

### *4.3. Ferroelectric–ferromagnetic composite structures with properties, sensitive to electric field*

Ferroelectric–ferromagnetic composite structures are of significant scientific and practical interest. In this case, there is a possibility to control magnetic characteristics by electric field. Numerous investigations show that in the single-phased systems, which display simultaneous existence of ferroelectric and magnetic orderings, either ferroelectric or magnetic component is weakened. What is more, temperature regions corresponding to maximum demonstration (level) of ferroelectricity and magnetism are tangibly separated from each other. This phenomenon, being of a fundamental nature [21], does not allow the development of bulk materials with the combination of features required in engineering. As a result, there is a great interest in the development of ferroelectric–ferromagnetic composite structures. In numerous cases, piezoelectric materials are used as a ferroelectric component [22].

In our work, for the first time it was suggested to use the materials, which display the positive temperature resistance coefficient (PTCR) effect, as a ferroelectric component. In this case, the coupling between electric and magnetic subsystems may occur by two ways. First, the PTCR materials are $n$-type semiconductors, while manganite-based materials, for example (La,Sr)$MnO_3$, are $p$-type semiconductors in a certain temperature range. Thus, a region of volume charge, which is sensitive to external electric field, may be formed at the interface PTCR/(La,Sr)$MnO_3$. Second, PTCR effect in the ferroelectric phase provides a high sensitivity of the properties to the action of electric field. Based on these ideas, layered structure PTCR/(La,Sr)$MnO_3$ was developed and investigated. Doped barium titanate ceramic plate was used as a substrate for (La,Sr)$MnO_3$ film (Fig. 4a). It is shown that the voltage applied to the substrate (between electrodes 1 and 2) gives rise to two effects: to the shift of the temperature of magnetic phase transition in the (La,Sr)$MnO_3$ film and reduction of its resistance (Fig. 4b). Such behavior can be explained by the sensitivity of doped barium titanate to external electric field and existence of magnetoelectric coupling between the PTCR substrate and (La,Sr)$MnO_3$ film. The

investigation shows exciting prospects for the development of electric field tuned composite structures with the use of ferroelectric materials displaying PTCR effect.

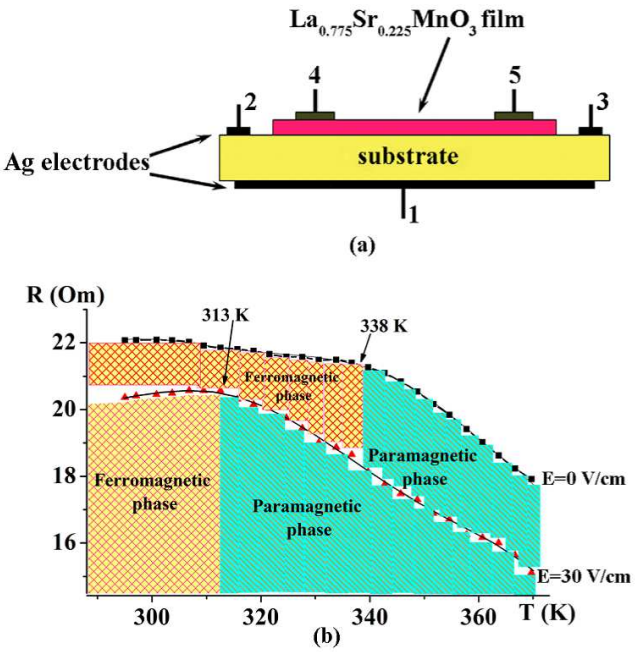


Fig. 4. (a) Structure based on (LaSr)$MnO_3$ film deposited on $Ba_{0.99}6Y_{0.004}TiO_3$ substrate: 1, 2, 3 — electrodes deposited on the substrate, 4, 5 — electrodes deposited on the film. (b) Temperature dependence of the electric resistance of (La,Sr)$MnO_3$ film deposited on the $Ba_{0.996}Y_{0.004}TiO_3$ substrate for different values of electric field applied to substrate (between electrodes 1–2).

### *4.4. Magnetocontrolled composite elements based on "dielectric resonator–ferrite film"*

Magnetocontrolled composite elements based on "dielectric resonator–ferrite film" can find wide technical applications. It is known that in development of radio-filters, solid-state generators, dielectric antennas, which are used in modern communication systems, thermostable high-$Q$ dielectric resonators play very important role [23]. Dielectric resonators are developed based on materials, which are characterized by the increased dielectric permittivity ($\varepsilon \approx 20$–$100$), low dielectric losses ($\tan\delta \approx 10^{-3}$–$10^{-4}$) and high thermal stability of electrophysical properties (temperature coefficient of dielectric permeability $TC\varepsilon \approx 10^{-5}$–$10^{-6}$ $K^{-1}$) [24] in the MW range. One of the drawbacks of high-$Q$ resonators is their inability to change the properties under external fields. It is known that, being combined with ferromagnets, dielectric resonators may attain magnetic field tunability [25]. However, ferromagnets introduce additional magnetic losses in the system, so the presence of large amount of ferromagnetic material makes it difficult to achieve characteristics required for modern communication systems. One of the ways to tackle this issue is the development of composite resonant elements, which include the high-$Q$ thermostable dielectric resonator and ferromagnetic film deposited on it. Such tunable elements were developed based on the barium tetratitanate dielectric resonators. It is shown that they are characterized by the high dielectric characteristics in the MW range ($\varepsilon = 35$, $TC\varepsilon \approx 2 \times 10^{-6}$ $K^{-1}$, $Q = 6000$). Nickel ferrite film with the spinel structure was deposited on the dielectric resonator by screen-printing from previously synthesized nanoparticles [25].

Composite resonator consisted of the dielectric resonator (diameter is 6.45 mm and height is 1.7 mm) and nickel ferrite film (thickness is 100 $\mu$m). As shown in Fig. 5, the field-induced frequency shift was 29 MHz in the vicinity of 11.6 GHz.

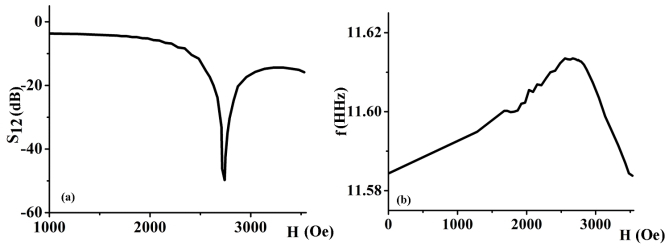


Fig. 5. Modification of the nickel ferrite-dielectric resonator transmission coefficient (a) and shift of the central resonant frequency (b) with applied external magnetic field.

### *4.5. Composite materials, which have the giant magnetocaloric effect, based on ferromagnetic film/ferroelectric*

Giant magnetocaloric effect in $La_{0.7}Ca_{0.3}MnO_3$/$BaTiO_3$ system. Magnetocaloric effects have been known since the nineteenth century, and their ability to provide mK temperatures was recognized via the award of 1949 Nobel prize in chemistry [26]. Half a century later, the 1997 discovery of large magnetocaloric effects near room temperature [27] led to suggestions for everyday applications in refrigeration and air-conditioning. Unfortunately, only few materials possess suitable magnetostructural transition parameters. It is therefore interesting to investigate whether a magnetic material showing small magnetocaloric effects can be forced to display large magnetocaloric effects by a second material to which it is coupled via strain. Keeping in mind this idea, the observation of giant extrinsic magnetocaloric effect was achieved in epitaxial films of the ferromagnetic manganite $La_{0.7}Ca_{0.3}MnO_3$ (LCMO) using strain-mediated feedback from $BaTiO_3$ (BTO) substrates near a first-order structural phase transition of the latter [28].

The manganite $La_{1-x}Ca_xMnO_3$ has attracted great attention after the 1994 discovery of colossal magnetoresistance [1], but it shows only small magnetocaloric effects

near the Curie temperature $T_C \approx 250$ K [28]. It adopts a perovskite structure and may therefore be grown epitaxially on a perovskite substrate of barium titanate BTO, which shows structural phase transitions at $\approx$ 200 K, $\approx$ 300 K and $\approx$ 400 K. The $\approx$ 200 K transition lies below the LCMO Curie temperature, and therefore strain from this transition in the substrate can influence the film in its ferromagnetic state

Macroscopic magnetometry data confirmed the expected ferromagnetism of LCMO/BTO, and revealed a jump in film magnetization due to strain from the $\approx$ 200 K transition in the substrate (Fig. 6). Similar jumps were also observed for $La_{0.7}Sr_{0.3}MnO_3$ (LSMO) films on BTO substrates, but detailed investigation showed that these jumps arise due to the rotation of magnetic domains [28]. By contrast, for LCMO/BTO, the rhombohedral to orthorhombic (R–O) transition modifies the magnitude of the local magnetization and therefore film entropy.

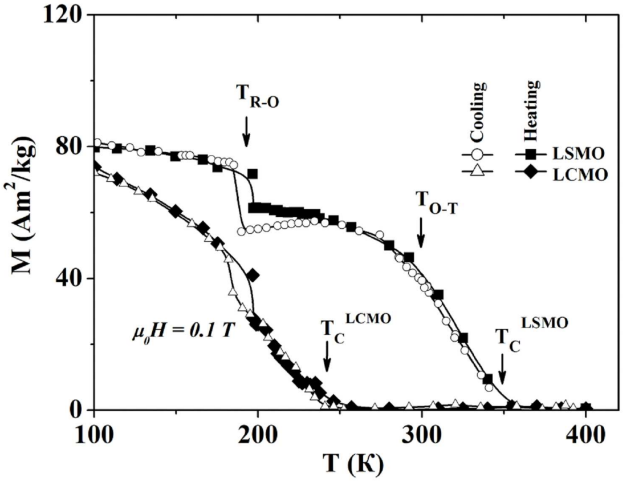


Fig. 6. Magnetization $M$ vs. temperature $T$ measured in $\mu_0 H = 0.1$ T on cooling (blue symbols) and heating (red symbols), showing magnetic jumps near $T_{R-O} \approx 200$ K below film Curie temperatures ($\approx 350$ K for LSMO/BTO and $\approx 240$ K for LCMO/BTO) [28].

Magnetic resonance studies showed that magnetic state of LCMO film is characterized by a coexistence of ferromagnetic and paramagnetic regions. Additionally, these measurements made it possible to separate the signals from ferromagnetic and paramagnetic phases, and trace the behavior of each. Figure 7 shows temperature dependences of the resonance field (a) and intensity of resonance absorption (b) for the ferromagnetic phase. The intensity of the FMR line is related to the volume fraction of ferromagnetic phase, while resonance field — to effective magnetization $M$ of this phase. It follows from these data that the ferromagnetic regions show a jump in volume fraction and not magnetization (temperature dependence of $M$ calculated from $H_{res}(T)$ data is shown in the inset of Fig. 7a).

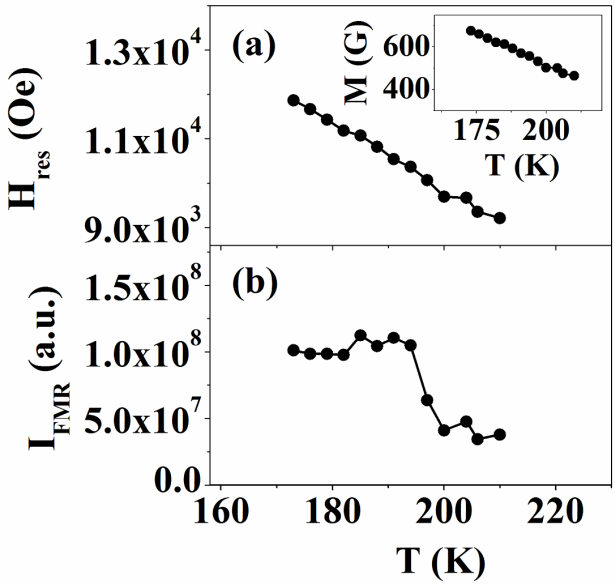


Fig. 7. Resonance field (a) and intensity of resonance absorption (b) vs. temperature for the ferromagnetic phase of the LCMO/BTO film. Inset in part (a) shows temperature dependence of magnetization calculated from the resonance field.

Having observed that the entropic jump in film magnetization can be driven by changing temperature, next step was to study whether it can also be driven by a magnetic field to yield a magnetocaloric effect. It was found that a magnetic field could drive the film directly from the low-magnetization state to the high-magnetization state. This demonstrated a strain-mediated feedback mechanism between the magnetic film and substrate.

At a certain temperature $T$, the isothermal entropy change $\Delta S(H)$ of a magnetic material due to applied magnetic field $H$ may be obtained via the Maxwell relation $\mu_0^{-1}(\partial S/\partial H)_T = (\partial M/\partial T)_H$ using

$$\Delta S\,(H) = \mu_0 \int_0^H \left(\frac{\partial M}{\partial T}\right)_{H'} \mathrm{d}H', \qquad (1)$$

provided that thermally driven changes in measured magnetization $M$ arise due to changes in the magnitude and not the direction of the local magnetization ($\mu_0$ is the permeability of free space). Therefore large gradients in $M(T)$ signify but do not generically guarantee giant MC effects. Using this indirect method, $\Delta S(H)$ is typically determined from a set of magnetization $M(H)$ isotherms. A number of direct caloric measurements have proved the validity of this indirect method [29].

The extrinsic reversible magnetocaloric effect in LCMO/BTO film was quantified using Eq. (2). It was found that near $T_{R-O}$, there is an isothermal entropy change of 9 J K$^{-1}$ kg$^{-1}$ due to a change in applied field corresponding to 1 T. The giant value of $|\Delta S/\mu_0 \Delta H| \approx$ 9 J K$^{-1}$ kg$^{-1}$ T$^{-1}$ corresponds to an isothermal heat change per unit field of $|\Delta Q/\mu_0 \Delta H| \approx 1700$ J kg$^{-1}$ T$^{-1}$,

and an adiabatic temperature change per unit field of $|\Delta T/\mu_0 \Delta H| = \mu_0^{-1} \mathrm{d}T_0/\mathrm{d}H \approx 0.4$ K T$^{-1}$. It should be noted that at $T_C^{LCMO}$, the much smaller intrinsic MC effect of 0.7 J K$^{-1}$ kg$^{-1}$ T$^{-1}$ was observed.

The demonstration with epitaxial films may in practice lead to the development of giant magnetocaloric materials based on alternative geometries with comparable volume fractions and a large interfacial area, e.g. core-shell nanoparticles or nanocomposites. It will also be attractive to explore alternative combinations of materials, in order to develop magnetocaloric effects at various operating temperatures in magnetic materials that have hitherto appeared highly unpromising.

## 5. Conclusions

Weakly agglomerated single-domain magnetic nanoparticles $MnFe_2O_4$ (M = Fe, Zn, Co, Mn, Ni) with the spinel structure and (La,Sr)$MnO_3$ with the perovskite structure were synthesized. It was shown that crystalline nanoparticles with the spinel structure form during the synthesis while in the case of synthesis of nanoparticles with perovskite structure an amorphous powder firstly is obtained. Therefore, the additional high-temperature treatment is necessary to obtain crystalline (La,Sr)$MnO_3$ nanoparticles.

Thin ferromagnetic LCMO and LSMO films with the thickness of 34±2 nm for LCMO and 55±5 nm for LSMO were obtained by pulsed laser deposition method. They were used for development of the composite elements, which have the giant magnetocaloric effect. (La,Sr)$MnO_3$ films with the thickness of 250–500 nm were synthesized via sol–gel method, and they were used for development of tunable elements.

It was shown that synthesized magnetic nanoparticles are promising as the mediators for magnetic hyperthermia treatment. Obtained ferromagnetic films may find application for development of the left-handed media and composite materials whose properties can be controlled by the external magnetic or electric fields.

## References


[1] R. von Helmolt, J. Wecker, B. Holzapfel, L. Schultz, K. Samwer, *Phys. Rev. Lett.* **71**, 2331 (1993).

[2] K.H. Graham, *MRS Bull.* **17**, 26 (1992).

[3] D.B. Williams, *The Transition Electron Microscope*, Springer Science+Business Media, New York 1996.

[4] L. Li, W. Jiang, K. Luo, H. Song, F. Lan, Y. Wu, Z. Gu, *Theranostics* **3**, 595 (2013).

[5] O. Veiseh, J.W. Gunn, M. Zhang, *Adv. Drug Deliv. Rev.* **62**, 284 (2010).

[6] B. Thiesen, A. Jordan, *Int. J. Hypertherm.* **24**, 467 (2008).

[7] B.L. Cushing, V.L. Kolesnichenko, C.J. O'Connor, *Chem. Rev.* **104**, 3893 (2004).

[8] D. Peddis, F. Orrum, A. Ardu, C. Cannas, A. Musinu, G. Piccaluga, *Chem. Mater.* **24**, 1062 (2012).

[9] M. Veverka, K. Zaveta, O. Kaman, P. Veverka, K. Knızek, E. Pollert, M. Burian, P. Kaspar, *J. Phys. D Appl. Phys.* **47**, 065503 (2014).

[10] L.A. Reznitskii, A.S. Guzei, *Russ. Chem. Rev.* **47**, 99 (1978).

[11] I.I. Caneva, D.G. Kratogin, V.G. Andreev, L.M. Letyuk, *Ferrite Materials and Components Magnetoelectronics*, MISIS, Moscow 2005.

[12] D.L. Leslie-Pelecky, R.D. Rieke, *Chem. Mater.* **8**, 1770 (1996).

[13] S. Morup, M.F. Hansen, C. Frandsen, *Compr. Nanosci. Technol.* **1**, 437 (2011).

[14] P. Dey, T.K. Nath, *Appl. Phys. Lett.* **89**, 163102 (2006).

[15] V.M. Kalita, A.I. Tovstolytkin, S.M. Ryabchenko, O.V. Yelenich, S.O. Solopan, A.G. Belous, *Phys. Chem. Chem. Phys.* **17**, 18087 (2015).

[16] O. Shydlovska, N. Zholobak, S. Dybkova, S. Osinsky, L. Bubnovskaya, O. Yelenich, S. Solopan, A. Belous, *Eur. J. Nanomed.* **9**, 33 (2014).

[17] L. Bubnovskaya, A. Belous, S. Solopan, A. Kovelskaya, L. Bovkun, A. Podoltsev, I. Kondtratenko, S. Osinsky, *J. Nanopart.* **2014**, 278761 (2014).

[18] T. Goto, A.V. Dorofeenko, A.M. Merzlikin, A.V. Baryshev, A.P. Vinogradov, M. Inoue, A.A. Lisyansky, A.B. Granovsky, *Phys. Rev. Lett.* **101**, 113902 (2008).

[19] M.K. Khodzitsky, T.V. Kalmykova, S.I. Tarapov, D.P. Belozorov, A.M. Pogorily, A.I. Tovstolytkin, A.G. Belous, S.A. Solopan, *Appl. Phys. Lett.* **95**, 082903 (2009).

[20] M.K. Khodzitsky, S.I. Tarapov, D.P. Belozorov, A.M. Pogorily, A.I. Tovstolytkin, A.G. Belous, S.A. Solopan, *Appl. Phys. Lett.* **97**, 131912 (2010).

[21] R. Ramesh, N.A. Spaldin, *Nature Mater.* **6**, 21 (2007).

[22] D.A. Filippov, M.I. Bichurin, V.M. Petrov, V.M. Laletin, G. Scrinivasan, *Phys. Solid State* **46**, 1674 (2004).

[23] C. Wang, K.A. Zaki, *IEEE Microwave Mag.* **8**, 115 (2007).

[24] A.G. Belous, O.V. Ovchar, M. Macek-Krzmanc, M. Valant, *J. Eur. Ceram. Soc.* **26**, 3733 (2006).

[25] I.V. Zavislyak, M.A. Popov, E.D. Solovyova, S.A. Solopan, A.G. Belous, *Mater. Sci. Eng. B* **197**, 36 (2015).

[26] The Nobel Prize in Chemistry 1949.

[27] V.K. Pecharsky, K.A. Gschneidner, *Phys. Rev. Lett.* **78**, 4494 (1997).

[28] X. Moya, L.E. Hueso, F. Maccherozzi, A.I. Tovstolytkin, D.I. Podyalovskii, C. Ducati, L.C. Philips, M. Ghidini, O. Hovorka, A. Berger, M.E. Vickers, E. Defay, S.S. Dheshi, N.D. Mathhur, *Nature Mater.* **12**, 52 (2013).

[29] L. Caron, Z.Q. Ou, T.T. Nguyen, D.C. Thanh, O. Tegus, E. Bruck, *J. Magn. Magn. Mater.* **321**, 3559 (2009).